Meso- and Rac-[bis(3-phenyl-6-tert-butylinden-1-yl)dimethylsilyl]zirconium Dichloride: Precatalysts for the Production of Differentiated Polyethylene Products with Enhanced Properties

Kaitie A. Giffin, Virginie Cirriez, Orlando Santoro, Alexandre Welle, Evgueni Kirillov, Jean-Francois Carpentier

polymers

MDPI

Article

Meso- and *Rac*-[bis(3-phenyl-6-*tert*-butylinden-1-yl)dimethylsilyl] zirconium Dichloride: Precatalysts for the Production of Differentiated Polyethylene Products with Enhanced Properties

Kaitie A. Giffin [1,2], Virginie Cirriez [2], Orlando Santoro [1], Alexandre Welle [2], Evgueni Kirillov [1,*] and Jean-François Carpentier [1,*]

[1] Centre National de la Recherche Scientifique (CNRS), Institut des Sciences Chimiques de Rennes (ISCR), University of Rennes, UMR 6226, F-35042 Rennes, France; kaitie.giffin@totalenergies.com (K.A.G.); orlando.santoro@uninsubria.it (O.S.)

[2] Total Energies One Tech Belgium, Zone Industrielle Feluy C, B-7181 Seneffe, Belgium; virginie.cirriez@totalenergies.com (V.C.); alexandre.welle@totalenergies.com (A.W.)

* Correspondence: evgueni.kirillov@univ-rennes1.fr (E.K.); jean-francois.carpentier@univ-rennes1.fr (J.-F.C.)

Abstract: *Ansa*-zirconocene complexes are widely employed as precatalysts for olefin polymerization. Their synthesis generally leads to mixtures of their *rac* and *meso* isomers, whose separation is often problematic. In this contribution, we report on the synthesis of a novel silyl-bridged bis(indenyl)-based metallocene, and on the separation of its *rac* and *meso* isomers by simple recrystallization from toluene. The two complexes, activated by methylaluminoxane (MAO), have been used as precatalysts in ethylene/1-hexene copolymerization. Regardless of the reaction conditions, the *meso* complex outperformed its *rac* congener. A similar trend was observed by performing the process in the presence of the silica-supported versions of the complexes. This is remarkable, since *meso* metallocenes generally display lower activities than their *rac* analogues. Furthermore, the *meso* isomer generates polymer products that are more in line with the targets for the preparation of a bimodal PE grade made of a lower-MW high-density (HDPE) fraction and a higher-MW linear low-density (LLDPE) fraction.

Keywords: *ansa*-zirconocene; *rac*/*meso* isomers; dual site; bimodal polyethylene; short-chain branches

Citation: Giffin, K.A.; Cirriez, V.; Santoro, O.; Welle, A.; Kirillov, E.; Carpentier, J.-F. *Meso-* and *Rac*-[bis(3-phenyl-6-*tert*-butylinden-1-yl) dimethylsilyl]zirconium Dichloride: Precatalysts for the Production of Differentiated Polyethylene Products with Enhanced Properties. *Polymers* **2022**, *14*, 2217. https://doi.org/10.3390/polym14112217

Academic Editor: Muhammad Atiqullah

Received: 14 May 2022
Accepted: 27 May 2022
Published: 30 May 2022

1. Introduction

In the field of commodity polyethylene (PE), there is an ongoing demand for polyethylene products with enhanced properties. Ziegler–Natta catalysis provides highly processable products (under certain conditions, such as injection molding) due to their broad molecular weight distribution (MWD) and normal comonomer incorporation (short-chain branches concentrated in the lower-molecular-weight chains). On the other hand, metallocene catalysts afford products with a narrow MWD and a uniform distribution of short-chain branches [1–3]. Such products can be advantageous on the basis of improved mechanical properties; however, they are often accompanied by processing issues. One solution to circumvent this shortage is the production of bimodal polyethylene with an inverse comonomer incorporation (short-chain branches concentrated in the higher-molecular-weight chains) [4,5]. The lower-molecular-weight (MW) component improves product processability, while the high-MW component is known to enhance mechanical properties (i.e., strength and stiffness). Bimodal PE grade made of a lower-MW high-density (HDPE) fraction and a higher-MW linear low-density (LLDPE) fraction is a highly desirable commodity polymer due to its improved performance relative to monomodal PE in a variety of applications, including its use in damage-resistant pipes and in lighter-weight flexible packaging [6].

For the copolymerization of ethylene with an α-olefin, further improvements to the state-of-the-art can be achieved with the design of new catalyst combinations that result

in a higher-density split between the lower-MW and the higher-MW fractions (very low comonomer incorporation in the shorter chains vs. the longer chains). This can be achieved through the rational design of new metallocenes. In this context, there is great interest in discovering industrially relevant highly active metallocene catalysts that generate a low-molecular-weight PE product with very low comonomer incorporation.

When mixtures of *rac* and *meso* stereoisomers of a given *ansa*-bis(indenyl) zirconocene are used in the homo-/copolymerization of ethylene with an α-olefin comonomer (e.g., 1-hexene), a broader MWD and variable comonomer incorporation is observed in the generated polymer. From a practical point of view, these types of precatalyst mixtures can lead to a decrease in reproducibility and a lower degree of control in the design of the polymer architecture. The isolation of racemic metallocene from the *rac*/*meso* mixture is often targeted, as each stereoisomer generates homo-/copolymers with features distinct from one another, such as a specific MWD, comonomer incorporation, activity, and overall response to other reaction parameters. Previous investigations of *meso*- and *rac*-*ansa*-bis(indenyl) zirconocenes have typically found that the *rac* isomers are more active in ethylene polymerization and generate products with higher MWs compared to their *meso* counterparts [7,8].

In this study, we report the synthesis and isolation of both *rac* and *meso* complexes of a new silyl-bridged disubstituted bis(indenyl) zirconocene. Both isomers were tested in the copolymerization of ethylene/1-hexene, and the resulting copolymers were characterized on the basis of the MW, the MWD, and the comonomer incorporation. In contrast to previous studies [7,8], the *meso* isomer was found to be a significantly more active polymerization catalyst than the *rac* isomer. Furthermore, the *meso* isomer produces polymer products that are more in line with the targets outlined above for the low-MW high-density block of a bimodal copolymer.

2. Materials and Methods

General considerations. Unless otherwise stated, all manipulations were conducted under nitrogen atmosphere, using either Schlenk or glovebox techniques. Solvents were dried on molecular sieves (4Å and 13X, 1:1 ratio) and activated alumina using a solvent purification system, deoxygenated by nitrogen purging and stored over activated 4 Å molecular sieves. Glassware was oven-dried at 150 °C for >2 h. The synthesis of proligand 1 was developed in our laboratories [9], while its upscaling was conducted at MCN Co. All other chemicals were obtained from Acros Organics (Geel, Belgium), Alfa Aesar (Ward Hill, MA, USA), and Sigma Aldrich (St. Louis, MO, USA) and used as received. Precatalysts *meso*-2 and *rac*-2 were supported onto silica (from PQ, D50: 40 μ) (0.4 wt% Zr) and MAO (30 wt% solution in toluene; contains ca. 10 wt% of free $AlMe_3$), using previously reported procedure [9].

NMR spectra of all organic and organometallic compounds were recorded on a 400 MHz Bruker Avance instrument at room temperature in Teflon-valved NMR tubes. ^1H and ^{13}C NMR chemical shifts are reported in ppm vs. $SiMe_4$ (0.00), as determined by reference to the residual solvent peak. $^{13}C\{^1H\}$ NMR spectroscopic analyses of PE samples were recorded on an AM-500 Bruker spectrometer equipped with a cryoprobe using the following conditions: solutions of ca. 200 mg of polymer in 1,2,4-trichlorobenzene/C_6D_6 (5:1 *v*/*v*) mixture at 135 °C in 10 mm tubes; inverse-gated experiment; pulse angle: 90°; delay = 30 s; acquisition time: 1.25 s; number of scans = 240.

DSC measurements were performed on a SETARAM Instrumentation DSC 131 differential scan calorimeter at a heating rate of 10 °C/min; first and second runs were recorded after cooling to 30 °C; the melting and crystallization temperatures reported in tables were determined on the second run.

GPC analyses of PE samples were carried out in 1,2,4-trichlorobenzene at 135 °C using polystyrene standards for universal calibration.

*2.1. Synthesis of [Bis(3-phenyl-6-tert-butylinden-1-yl)dimethylsilyl]zirconium Dichloride (**2**)*

In a 500 mL round-bottom flask, to a solution of dimethyl bis[(3-phenyl-6-tert-butylinden-1-yl)]silane (**1**, 9.7 g, 552.8 g/mol, 0.0176 mol) in toluene (130 mL) was added *n*-BuLi (22.0 mL of a 1.6 M solution in hexanes, 0.0351 mol) over the course of 15 min. The color first changed from clear orange to dark red, then to a cloudy brown-beige just after the end of the addition. The mixture was left to stir at room temperature for 24 h. In a second 500 mL round-bottom flask, $ZrCl_4$ (4.1 g, 0.0176 mol) was suspended in toluene (50 mL). With stirring, THF (2.7 g, 0.0370 mol) was added dropwise over ca. 5 min. This reaction mixture was left to stir at room temperature for 2 h. The suspension of the dilithiated ligand was then added over the course of 15 min to the $ZrCl_4$/THF mixture. Extra THF (ca. 2 mL) was used to wash the white solid off the walls of the ligand dianion flask and ensure complete transfer. Over the course of the addition, the color changed to cloudy dark orange. The resulting mixture was left to stir at room temperature for 18 h and then filtered over a 75 mL POR3 frit packed with Celite (dried in the oven for 3 days prior to use). The reaction flask and Celite was washed with extra toluene (ca. 40 mL, until no orange color remained on the Celite). The filtrate was concentrated under vacuum to ca. 200 mL; an orange precipitate started to form on the walls of the flask. The flask was well sealed using silicone grease and a glass stopper, shipped out of the glovebox, and stored at −35 °C for 20 h. At this point, a significant amount of orange solid had precipitated. The flask was then left at room temperature to defrost, prior to returning to the glovebox. The mixture was filtered over a 75 mL POR4 frit, collecting a bright-orange solid and a red-orange filtrate. The solid was washed with pentane (2 × 3 mL), then dried on the frit for ca. 1.5 h. The solid was then transferred to a vial for storage: *Fraction #1*, 2.58 g (21% yield). The filtrate was concentrated under vacuum in a 500 mL round-bottom flask until an orange precipitate began to form. The flask was sealed with a greased stopper, shipped out of the glovebox, and stored at −35 °C for 20 h. The flask was defrosted at room temperature, returned to the glovebox, and the mixture was filtered over a POR4 frit, collecting a second fraction of bright-orange solid and an orange filtrate. The solid was washed with pentane (2 × 3 mL) and was left to dry under vacuum on the frit for 2 h. The solid was then transferred to a vial for storage: *Fraction #2*, 446 mg (4% yield). The *meso* purity of each fraction was determined by ^{1}H NMR spectroscopy. Fractions #1 and #2 had similar *meso* purities and could be combined, resulting in an overall yield of 25% with a 24:1 *meso*/*rac* ratio (see the Supporting Information, Figure S1).

Isomer *meso*-2: ^{1}H NMR (400 MHz, CD_2Cl_2, 25 °C; Figure S1, top): δ 7.56 (dd, 2H, J = 9.2, Ar-*H*); 7.62 (s, 2H, Ar-*H*); 7.53-7.51 (m, 4H, Ar-*H*); 7.40 (m, 4H, Ar-*H*); 7.28 (m, 2H, Ar-*H*); 7.09 (dd, 2H, J = 9.2, Ar-*H*); 6.05 (s, 2H, Cp-*H*); 1.43 (s, 3H, Si-C$H_{3(endo)}$); 1.25 (s, 18H, C(CH_3)$_3$); 0.94 (s, 3H, Si-C$H_{3(exo)}$). ^{13}C{^{1}H} NMR (CD_2Cl_2, 100 MHz, 25 °C; Figure S1, bottom): δ 151.8, 138.0, 135.1, 133.6, 129.3, 128.3, 126.3, 124.7, 119.9, 117.9, 86.9, 35.0, 30.8, 21.1, −0.59, −4.3.

Evaporation of the solvent from the mother solution and further recrystallization from pentane at room temperature afforded a *rac*-enriched product (30% yield, 1:6 *meso*/*rac* ratio, as determined by ^{1}H NMR spectroscopy, see the Supporting Information, Figure S2).

Isomer *rac*-**2**: ^{1}H NMR (400 MHz, CD_2Cl_2, 25 °C; Figure S2, top): δ 7.69 (dd, 2H, J = 9.0 Hz, Ar-*H*); 7.60 (s, 2H, Ar-*H*); 7.50-7.49 (m, 4H, Ar-*H*); 7.38 (m, 4H, Ar-*H*); 7.30 (m, 2H, Ar-*H*); 7.10 (dd, 2H, J = 9.0, Ar-*H*); 6.19 (s, 2H, Cp-*H*); 1.28 (s, 18H, C(CH_3)$_3$); 1.17 (s, 6H, Si-CH_3). ^{13}C{^{1}H} NMR (100 MHz, CD_2Cl_2, 25 °C; Figure S2, bottom): δ 152.3, 134.7, 131.8, 130.1, 129.2, 128.4, 127.3, 126.3, 125.9, 124.7, 118.6, 116.1, 87.1, 35.1, 30.9, −1.65.

APPI+-MS (toluene, *m*/*z*) [M]$^+$ Calcd for [$C_{40}H_{42}Cl_2SiZr$]$^+$: 712.1473. Found: 712.1473 (see the Supporting Information, Figure S3).

2.2. Ethylene (Co)Polymerization Reactions

2.2.1. Homogeneous Conditions

Polymerization tests were performed in triplicates in a 24-slot high-throughput screening reactor in 50 mL glass vials. Under nitrogen atmosphere, each vial was equipped with

a magnetic stir bar and loaded with *n*-heptane (25 mL), a toluene solution of the activated catalyst (200 µL, $[Al_{MAO}]/[Zr] = 1000$, $[Zr]_0 = 10$ µM), and the desired amount of 1-hexene. The vials were sealed with a crimp cap and introduced into the corresponding slots of the reactor, thermostated at 80 °C. The reactor was closed and pressurized with ethylene at the desired pressure (the gas was introduced in the vials through a needle piercing the septum of the crimp caps). The reaction was stopped after 15 min by venting the reactor. The polymer samples were collected and dried in air at room temperature for 16 h, and under reduced pressure at 50 °C for 3 h.

2.2.2. Heterogeneous Conditions

The tests were performed in a parallel reactor system integrating six 130 mL stainless steel reactors equipped with a thermocouple, a pressure transducer, and constant-pressure regulator. Each reactor featured an antechamber. Each vessel was loaded with iso-butane (75 mL), the desired amount of 1-hexene (0–3.0 wt%), H_2 (800 ppm), and ethylene (23.8 bar), and the temperature was equilibrated at 85 °C for 30 min. Each antechamber was charged with heptane (2 mL), the supported catalyst (2.0 mg), and the desired amount of TIBAL. The polymerizations were started by pressurizing these mixtures in the reactors, and were stopped after 1 h by venting the reactors. The polymer samples were collected and left to dry in air at room temperature overnight.

3. Results and Discussion

3.1. Metallocene Synthesis

The investigation was focused on silyl-bridged bis(indenyl)-based metallocenes, due to the industrial and academic relevance of such catalyst systems for olefin polymerization [10–13]. The new dimethylsilylene-bridged bis(indenyl) compound **1** was synthesized by using an adapted procedure based on a previously reported protocol [9]. The targeted zirconocene complexes ***meso*-2** and ***rac*-2** were synthesized by treating the dilithiated salts of proligand **1** with $ZrCl_4(THF)_2$ (formed in situ by the addition of two THF equivalents to $ZrCl_4$ in toluene, Scheme 1). This synthetic strategy is unselective towards either isomer and leads to a ca. 55/45 mixture of ***meso*/*rac*-2**, as determined by ^{1}H NMR analysis (see the Supporting Information). Due to the disparate solubility of the *rac* and *meso* isomers in toluene, it was possible to isolate the *meso* form by fractional crystallization in a 30% overall yield and with a *meso* purity of 96%. The work-up of the filtrate of this reaction affords a *rac*-enriched product (30% yield, 75% *rac* purity) [14].

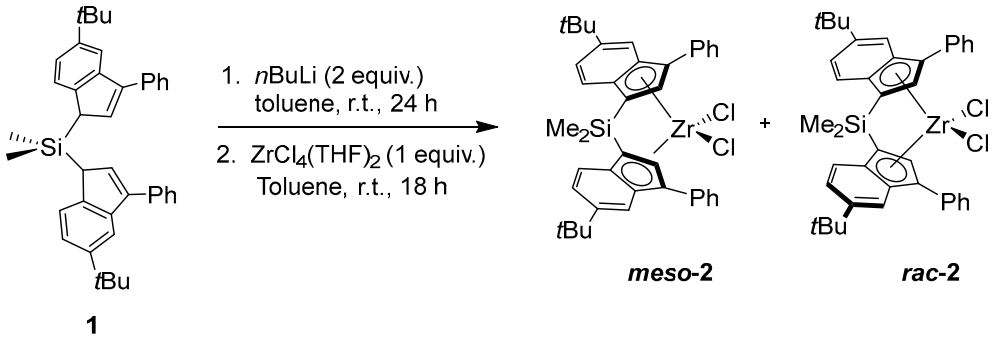

Scheme 1. Synthesis of *meso*- and *rac*-[bis(3-phenyl-6-*tert*-butylinden-1-yl)dimethylsilyl]zirconium dichloride (***meso*/*rac*-2**).

Though all of our attempts to obtain crystals of ***meso*-2** and ***rac*-2** isomers suitable for X-ray analysis failed, their possible structures were modeled by DFT computations. These calculations suggested the ***meso*-2** isomer to be slightly more stable (by 0.8 kcal·mol^{-1}). This energy difference with the ***rac*-2** form corresponds to a respective theoretical ratio of ca. 4:1 at room temperature. Note, however, that this minimal energy difference falls within

the accuracy of DFT computations usually accepted (2–3 kcal·mol^{-1}) and is therefore not inconsistent with the ca. 1:1 ratio observed experimentally.

For a better representation and comparison of the overall structures and steric hindrance around the metal center in each isomer, a set of regular descriptors was used, including the percentage of buried %V_{bur} volume [15] and Ind_{cent}–Zr–Ind_{cent} bite angles. The computed %V_{free} data (determined as %V_{free} = 100 − %V_{bur}) provide a measurement of the space available in the first coordination sphere of the metal center; steric maps were generated for a selected series of complexes (Scheme 2).

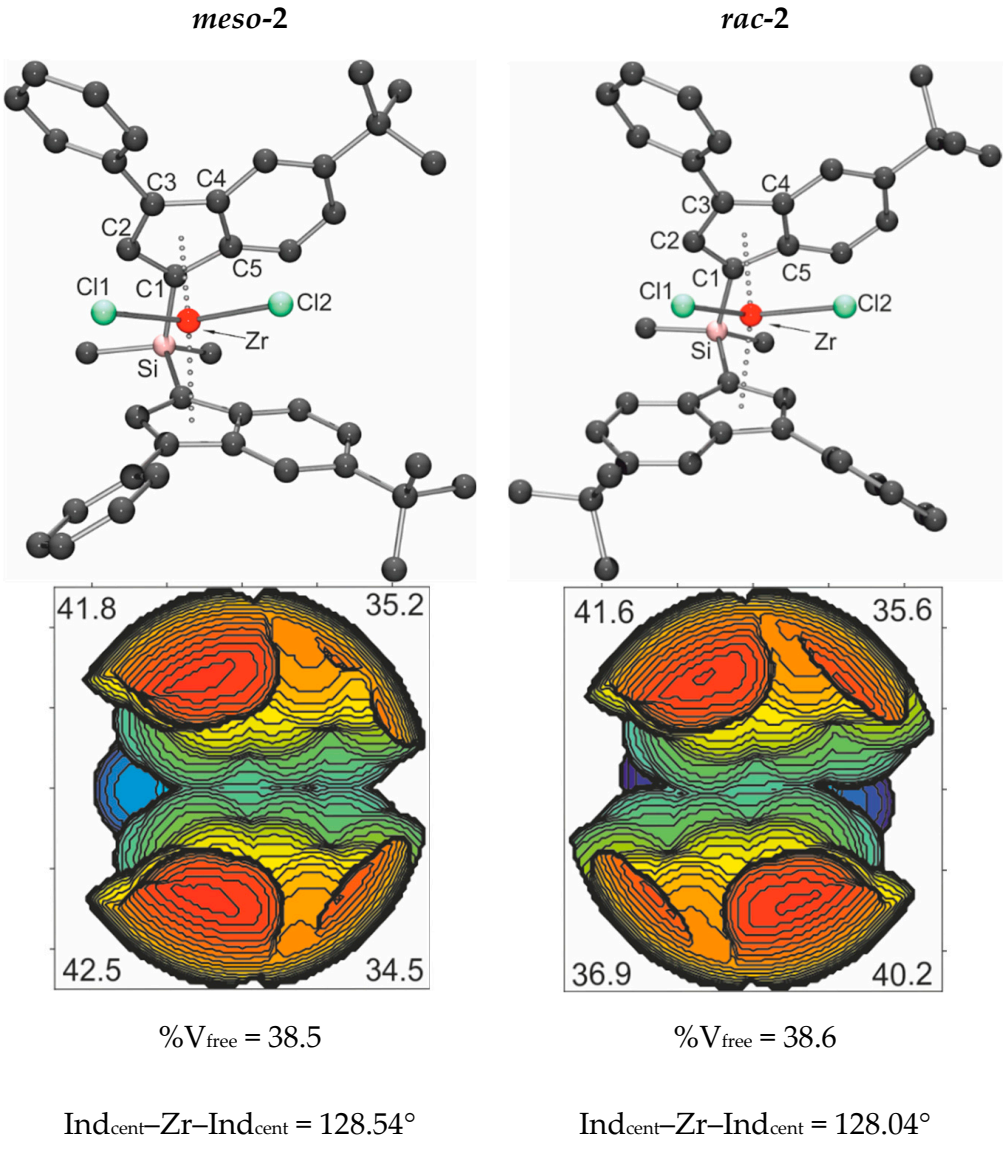

Scheme 2. Calculated data for ***meso*-2** and ***rac*-2** isomers: DFT-optimized structures, steric maps, and free volumes (%V_{free} = 100 − %V_{bur}), calculated for the entire molecules and for each quadrant, with sphere radius = 5.0 Å and Ind_{cent}–Zr–Ind_{cent} bite angles [°] as computed for the optimized geometries (see the Supporting Information for details).

The geometrical descriptors %V_{free} and the Ind_{cent}–Zr–Ind_{cent} angles in the molecules of both isomers are very similar. Therefore, essentially, the differences in the mutual organization of the corresponding quadrants in the metal coordination sphere may intrinsically influence the performances of these two isomers in ethylene/1-hexene copolymerization catalysis.

3.2. Copolymerization of Ethylene and 1-Hexene Catalyzed by Rac- and Meso-2 in Homogeneous Conditions

The compounds ***meso***- and ***rac*-2**, activated by methylaluminoxane (MAO), were tested as catalysts in the ethylene/1-hexene copolymerization (Table 1). Regardless of the amount of comonomer employed, the *meso*-**2**/MAO system proved ca. 3 times more productive than the *rac*-**2**-based analogue. Upon increasing the amount of 1-hexene, a progressive improvement in the catalysts' activity was observed. Such a beneficial comonomer effect is consistent with previous reports [16,17]. In the case of *meso*-**2**, higher comonomer concentrations led to a narrower MWD (from 5.7 to 3.1 for 0 wt% and 3.0 wt% of 1-hexene added, respectively), while, with *rac*-**2**, the MWD values were found in a very narrow range (3.3−3.5). The 1-hexene content in the final polymers was found to be proportional to the amount of comonomer employed in each run, with *rac*-**2** exhibiting a 1.5-fold higher comonomer incorporation ability than *meso*-**2**. Moreover, higher ethylene pressure proved to have a detrimental impact on 1-hexene incorporation only with the *rac*-based system (Table 1, cf. runs 9−10 and 11−12).

^{13}C NMR spectroscopy analysis of the polymers prepared with the *meso*-**2**/MAO system indicated the formation of ethyl branches, whose extent could be slightly reduced upon increasing the ethylene pressure (Table 1, cf. runs 1–2 and 9–10). The occurrence of this type of branching has been frequently observed with *meso*-type metallocenes (*vide infra*) and could originate from a regular chain-walking mechanism [18–22].

Table 1. Copolymerization of ethylene and 1-hexene catalyzed by homogeneous *meso- and rac*-**2**/MAO catalyst systems [a].

Run	Complex	C6$_{(add.)}$ [b] [wt%]	Activity [c] [kg/g·h]	T_m [d] [°C]	M_n [e] [kDa]	M_w [e] [kDa]	MWD [e]	C6$_{(incorp.)}$ [f] [wt%]	Ethyl Branches [f,g] [wt%]
1	***meso*-2**	0.0	140	125	7.0	37.8	5.7	0.0	5.9
2 [h]			100	125	4.6	14.0	3.0	0.0	3.7
3	***rac*-2**		44	129	13.7	45.5	3.3	0.0	0.3
4 [h]			80	130	15.2	43.4	2.9	0.0	0.1
5	***meso*-2**	0.7	176	121	6.3	26.6	4.2	1.5	4.2
6	***rac*-2**		60	128	12.3	39.6	3.2	2.2	0.4
7	***meso*-2**	1.3	188	120	6.0	21.9	3.6	2.8	4.1
8	***rac*-2**		64	126	11.1	35.7	3.2	3.4	0.4
9	***meso*-2**	2.5	200	122	4.6	13.0	2.8	2.8	2.8
10 [h]			112	123	4.1	11.4	2.8	2.7	2.2
11	***rac*-2**		72	124	10.3	34.5	3.3	4.9	0.4
12 [h]			88	126	11.4	33.0	2.9	1.4	0.1
13	***meso*-2**	3.0	208	118	5.6	17.7	3.1	5.5	4.8
14	***rac*-2**		72	123	9.8	34.4	3.5	7.9	0.5

[a] Reaction conditions: 25 mL heptane, [Zr]0 = 10 μM, AlMAO/Zr = 1000, T = 70 °C, ethylene pressure = 15 bar, 15 min. [b] With respect to heptane. [c] Expressed as kg of (co)polymer/g of metallocene per h. [d] Determined by DSC. [e] Determined by GPC; MWD = Mw/Mn. [f] Determined by 13C NMR spectroscopy; C6 = 1-hexene. [g] Expressed as wt% of 1-butene incorporated [23] [h]. Ethylene pressure = 25 bar.

3.3. Copolymerization of Ethylene with 1-Hexene Catalyzed by Heterogeneous Silica-Supported Rac- and Meso-2

The silica-supported versions of both isomers of the metallocene, namely, **supp-*meso*-2** and **supp-*rac*-2**, were tested as catalysts in the ethylene/1-hexene copolymerization (Table 2). As observed under homogeneous conditions, **supp-*meso*-2** proved a much more productive polymerization catalyst than **supp-*rac*-2**, regardless of the amount of comonomer introduced. This is remarkable since, to date, only a limited number of *meso*-metallocenes have displayed higher catalytic activity than their corresponding *rac*-isomers [24,25]. It is tentatively proposed that such difference could arise either from a faster deactivation of the *rac*

complex, possibly due to the formation of dormant heterobimetallic Al/Zr species [26–28], or to the occurrence, for the *meso* isomer, of a "stationary chain" polymerization mechanism, in which the monomer coordinates the active center always from the same (more accessible) side [24,29].

Table 2. Copolymerization of ethylene and 1-hexene with heterogeneous **supp-*meso*-2** and **supp-*rac*-2** [a].

Entry	Supp-Cat	C6$_{(added)}$ [b] [wt%]	Activity [c] [kg/g·h]	T_m [d] [°C]	M_n [e] [kDa]	M_w [e] [kDa]	MWD [e]	C6$_{(incorp.)}$ [f] [wt%]	Ethyl Branches [f,g] [wt%]
1	*meso*-2	0	4.5	129	10.2	29.4	2.9	0	1.8
2	*rac*-2		1.1	130	10.3	29.7	2.9	0	1.0
3	*meso*-2	0.7	4.3	129	10.1	29.0	2.9	≤0.1	1.9
4	*rac*-2		1.3	127	10.2	27.7	2.7	1.0	1.0
5	*meso*-2	1.5	4.4	128	9.9	28.4	2.9	0.2	1.9
6	*rac*-2		1.4	127	10.5	31.1	3.0	2.1	0.9
7	*meso*-2	2.3	4.3	129	9.9	28.6	2.9	0.2	1.9
8	*rac*-2		1.2	126	10.5	31.1	3.0	2.1	0.9
9	*meso*-2	3.0	4.5	129	9.9	28.2	2.9	0.2	1.9
10	*rac*-2		1.6	126	10.7	33.7	3.2	2.6	0.8

[a] Reaction conditions: 75 mL isobutane, 100 ppm triisobutylaluminum, 800 ppm H_2, T_{polym} = 85 °C, ethylene pressure = 23.8 bar. [b] With respect to isobutane. [c] Expressed as kg of (co)polymer/g of metallocene per h. [d] Determined by DSC. [e] Determined by GPC; MWD = M_w/M_n. [f] Determined by ^{13}C NMR spectroscopy. [g] Expressed as wt% of 1-butene incorporated [23].

A screening with varying 1-hexene content was subsequently performed to further explore the comonomer incorporation ability of the two catalysts (entries 3−10). For **supp-*meso*-2**, no significant differences were observed in terms of the productivity and polymer properties (MW, MWD, and melting-temperature values) when the weight % of 1-hexene added was increased from 0 to 3.0 wt%. **Supp-*rac*-2** also proved capable of incorporating 1-hexene, albeit to a much lesser extent than its homogeneous version. The difference between the comonomer incorporation abilities of the homogeneous and supported versions of ***meso*-** and ***rac*-2** could be explained in terms of the accessibility of the metal center. In fact, in the heterogenized system, one face of the metallocene is hindered by the support, which hampers the coordination/insertion of larger monomers (i.e., 1-hexene or macromonomers) [16,30].

The formation of ethyl branches was observed with both catalyst systems, albeit to a greater extent in the case of **supp-*meso*-2**. The origin of ethyl-branch formation and the metallocene/bis(indenyl) substituent effects on the ethyl-branch content has been studied in detail by Oliva et al.; their combined experimental/theoretical study supports a mechanism in which β-hydride transfer to the coordinated monomer, followed by insertion of the unsaturated chain into the generated Zr−C(ethyl) bond, is competitive with regular chain propagation [18–22].

4. Conclusions

The metalation of the silyl-bridged bis(indenyl) proligand **1** afforded an almost equimolar mixture of the corresponding dichlorozirconocene complexes, namely, the *rac*-**2** and *meso*-**2** isomers. Although attempted selective synthetic approaches towards the *rac*- and *meso*-complexes were unsuccessful, the two isomers could be separated by recrystallization from toluene. When activated by methylaluminoxane, both complexes proved productive in the ethylene/1-hexene copolymerization, both under homogeneous and slurry conditions. Remarkably and unlike the common literature trends, *meso*-**2** was found to be ca. 3 times more productive than its racemic counterpart. This was tentatively accounted to a possible faster deactivation of *rac*-**2**, or to the occurrence of a "*stationary chain*" *polymerization mechanism* with *meso*-**2**. Further mechanistic studies along these lines are underway.

Moreover, polymerization studies for dual-site catalyst combinations that incorporate the new *meso*-bis(indenyl) zirconocene are planned.

Supplementary Materials: The following supporting information can be downloaded at: https://www.mdpi.com/article/10.3390/polym14112217/s1, Metallocene synthesis, Figure S1: ^{1}H (400 MHz, top) and ^{13}C{^{1}H} (100 MHz, bottom) NMR spectra (CD_2Cl_2, 25 °C) of isolated *meso*-**2**; Figure S2: ^{1}H (400 MHz, top) and ^{13}C{^{1}H} (400 MHz, bottom) NMR spectra (CD_2Cl_2, 25 °C) of the *rac*-enriched complex **2**; Figure S3: APPI+-MS spectrum of *rac*-**2**; Attempted *racemo*- and *meso*-selective metallocene synthesis; Figure S4: ^{1}H NMR spectrum (CD_2Cl_2, 400 MHz, 25 °C) of the crude reaction mixture indicating *rac*-**3** as the major product; Figure S5: ^{1}H NMR spectrum (400 MHz, CD_2Cl_2, 25 °C) of the crude reaction mixture between **3** and Me_2SiCl_2 affording complex **2** in ca. 4:1 *rac/meso* ratio; Figure S6: Aromatic region of the ^{1}H NMR spectrum (400 MHz, CD_2Cl_2, 25 °C) of the crude reaction mixture resulting from the attempted *meso*-selective synthesis of complex **2**, indicating the presence of both *rac*- and *meso* isomers (ca. 1:1 ratio), as well as unreacted ligand **1**; Figure S7: ^{13}C{^{1}H} NMR spectrum (100 MHz, TCB/C_6D_6, 135 °C) of a PE synthesized with *meso*-**2** in the absence of 1-hexene (Table 1, entry 1); Figure S8: ^{13}C{^{1}H} NMR spectrum (100 MHz, TCB/C_6D_6, 135 °C) of a PE copolymer synthesized with *meso*-**2** in the presence 3.0 wt% of 1-hexene (Table 1, entry 13); Figure S9: GPC traces of the PEs made with **supp-*rac*-2** (orange) and **supp-*meso*-2** (blue) (Table 2, entries 1 and 2); Figure S10: GPC traces of the PEs prepared with **supp-*meso*-2** in the presence of difference amounts of 1-hexene (Table 2, entries 3, 5, 7, and 9): all curves are perfectly overlapped; Computational Studies; Cartesian coordinates [31–38].

Author Contributions: V.C., A.W., E.K. and J.-F.C. designed the study and the experiments. K.A.G. and O.S. performed the experiments and analyses. K.A.G., O.S., J.-F.C. and E.K. interpreted the experiments and wrote the manuscript. A.W. and V.C. helped with the cosupervision of the study. All authors have read and agreed to the published version of the manuscript.

Funding: This research received no external funding.

Institutional Review Board Statement: Not applicable.

Informed Consent Statement: Not applicable.

Data Availability Statement: Not applicable.

Acknowledgments: We are grateful to Katty Den Dauw for assistance in NMR analyses. E.K. thanks ENSCR and the CTI group of ISCR for the computational facilities.

Conflicts of Interest: The authors declare no conflict of interest.

References and Notes

1. Tso, C.C.; DesLauriers, P.J. Comparison of methods for characterizing comonomer composition in ethylene 1-olefin copolymers: 3D-TREF vs. SEC-FTIR. *Polymer* **2004**, *45*, 2657–2663. [CrossRef]
2. Li, C.; Shan, P.; Soares, J.B.P.; Penlidis, A. Mechanical properties of ethylene/1-hexene copolymers with tailored short chain branching distributions. *Polymer* **2002**, *43*, 767. [CrossRef]
3. Shamiri, A.; Chakrabarti, M.H.; Jahan, S.; Hussain, M.A.; Kaminsky, W.; Aravind, P.V.; Yehye, W.A. The Influence of Ziegler-Natta and Metallocene Catalysts on Polyolefin Structure, Properties, and Processing Ability. *Materials* **2014**, *7*, 5069–5108. [CrossRef] [PubMed]
4. Cicmil, D.; Meeuwissen, J.; Vantomme, A.; Wang, J.; van Ravenhorst, I.K.; van der Bij, H.E.; Muñoz-Murillo, A.; Weckhuysen, B.M. Polyethylene with Reverse Co-monomer Incorporation: From an Industrial Serendipitous Discovery to Fundamental Understanding. *Angew. Chem. Int. Ed.* **2015**, *54*, 13073–13079. [CrossRef]
5. Böhm, L.L.; Enderle, H.F.; Fleißner, M. High-density polyethylene pipe resins. *Adv. Mater.* **1992**, *4*, 234–238. [CrossRef]
6. Scheirs, J.; Böhm, L.L.; Boot, J.C.; Leevers, P.S. PE100 Resins for Pipe Applications: Continuing the Development into the 21st Century. *Trends Polym. Sci.* **1996**, *4*, 408–415.
7. Arnold, T.A.Q.; Buffet, J.-C.; Turner, Z.R.; O'Hare, D. Synthesis, characterisation, and polymerisation studies of hexamethylindenyl zirconocenes and hafnocenes. *J. Organomet. Chem.* **2015**, *792*, 55–65. [CrossRef]
8. Ransom, P.; Ashley, A.E.; Brown, N.D.; Thompson, A.L.; O'Hare, D. Synthesis, Characterization, and Polymerization Studies of Ethylenebis(hexamethylindenyl) Complexes of Zirconium and Hafnium. *Organometallics* **2011**, *30*, 800–814. [CrossRef]
9. Cirriez, V.; Welle, A.; Vantomme, A. Dual Catalyst Composition. Patent WO/2019/025528, 2 August 2018.
10. Brintzinger, H.H.; Fischer, D.; Mülhaupt, R.; Rieger, B.; Waymouth, R.M. Stereospecific Olefin Polymerization with Chiral Metallocene Catalysts. *Angew. Chem. Int. Ed. Engl.* **1995**, *34*, 1143–1170. [CrossRef]

11. Severn, J.R.; Chadwick, J.C.; Duchateau, R.; Friederichs, N. "Bound but Not Gagged" Immobilizing Single-Site α-Olefin Polymerization Catalysts. *Chem. Rev.* **2005**, *105*, 4073–4147. [CrossRef]
12. Kaminsky, W. The discovery of metallocene catalysts and their present state of the art. *J. Polym. Sci. A Polym. Chem.* **2004**, *42*, 3911–3921. [CrossRef]
13. Resconi, L.; Cavallo, L.; Fait, A.; Piemontesi, F. Selectivity in Propene Polymerization with Metallocene Catalysts. *Chem. Rev.* **2000**, *100*, 1253–1346. [CrossRef]
14. Attempts towards *rac*- and *meso*-selective synthesis were also carried-out. See the Supplementary Materials.
15. The SambVca 2.1 software was used to calculate $\%V_{bur}$ and generate steric maps:Falivene, L.; Cao, Z.; Petta, A.; Serra, L.; Poater, A.; Oliva, R.; Scarano, V.; Cavallo, L. Towards the online computer-aided design of catalytic pockets. *Nat. Chem.* **2019**, *11*, 872–879. [CrossRef]
16. Galland, G.B.; Seferin, M.; Mauler, R.S.; Dos Santos, J.H.Z. Linear low-density polyethylene synthesis promoted by homogeneous and supported catalysts. *Polym. Int.* **1999**, *48*, 660–664. [CrossRef]
17. Wu, Q.; García-Peñas, A.; Barranco-García, R.; Cerrada, M.L.; Benavente, R.; Pérez, E.; Gómez-Elvira, J.M. A New Insight into the Comonomer Effect through NMR Analysis in Metallocene Catalysed Propene–*co*–1-Nonene Copolymers. *Polymers* **2019**, *11*, 1266. [CrossRef]
18. Melillo, G.; Izzo, L.; Zinna, M.; Tedesco, C.; Oliva, L. Branching Formation in the Ethylene Polymerization with Meso Ansa Metallocene-Based Catalysts. *Macromolecules* **2002**, *35*, 9256–9261. [CrossRef]
19. Melillo, G.; Izzo, L.; Centore, R.; Tuzi, A.; Voskoboynikov, A.Z.; Oliva, L. meso-$Me_2Si(1\text{-indenyl})_2ZrCl_2$/methylalumoxane catalyzed polymerization of the ethylene to ethyl-branched polyethylene. *J. Mol. Catal. A-Chem.* **2005**, *230*, 29–33. [CrossRef]
20. Caporaso, L.; Galdi, N.; Oliva, L.; Izzo, L. Tailoring the Metallocene Structure to Obtain LLDPE by Ethene Homopolymerization: An Experimental and Theoretical Study. *Organometallics* **2008**, *27*, 1367–1371. [CrossRef]
21. Schwerdtfeger, E.D.; Irwin, L.J.; Miller, S.A. Highly Branched Polyethylene from Ethylene Alone via a Single Zirconium-Based Catalyst. *Macromolecules* **2008**, *41*, 1080–1085. [CrossRef]
22. Izzo, L.; Puranen, A.T.; Repo, T.; Oliva, L. Comparison of the C_1-symmetric diastereoisomers of a zirconocene-based catalyst in ethylene polymerization: A benzyl substituent as a regulator in branch formation. *J. Polym. Sci. A* **2006**, *44*, 3551–3555. [CrossRef]
23. The amount of ethyl branches expressed in terms of wt% of 1-butene wt% is given strictly as a value for comparison to 1-hexene wt% incorporated, and it is not meant to infer that the generated ethyl branches are a result of *in situ* butene formation.
24. Vathauer, M.; Kaminsky, W. Homopolymerizations of α-Olefins with Diastereomeric Metallocene/MAO Catalysts. *Macromolecules* **2000**, *33*, 1955–1959. [CrossRef]
25. Schaverien, C.J.; Ernst, R.; Schut, P.; Skiff, W.M.A.; Resconi, L.; Barbassa, E.; Balboni, D.; Dubitsky, Y.A.; Orpen, A.G.; Mercandelli, P.; et al. New Class of Chiral Bridged Metallocene: Synthesis, Structure, and Olefin (Co)polymerization Behavior of rac- and meso-1,2-$CH_2CH_2\{4\text{-}(7\text{-Me-indenyl})\}_2ZrCl_2$. *J. Am. Chem. Soc.* **1998**, *120*, 9945–9946. [CrossRef]
26. Tisse, V.F.; Boisson, C.; McKenna, T.F.L. Activation and Deactivation of the Polymerization of Ethylene over *rac*-$EtInd_2ZrCl_2$ and $(n\text{BuCp})_2ZrCl_2$ on an Activating Silica Support. *Macromol. Chem. Phys.* **2014**, *215*, 1358–1369. [CrossRef]
27. Bochmann, M.; Lancaster, S.J. Monomer–Dimer Equilibria in Homo- and Heterodinuclear Cationic Alkylzirconium Complexes and Their Role in Polymerization Catalysis. *Angew. Chem. Int. Ed.* **1994**, *33*, 1634–1637. [CrossRef]
28. Song, F.; Cannon, R.D.; Bochmann, M. Zirconocene-Catalyzed Propene Polymerization: A Quenched-Flow Kinetic Study. *J. Am. Chem. Soc.* **2003**, *125*, 7641–7653. [CrossRef]
29. Albeit plausible, such hypothesis remains unlikely since such mechanism is commonly considered for the polymerization of higher olefines (1-butene and 1-pentene).
30. Santoro, O.; Piola, L.; Mc Cabe, K.; Lhost, O.; Den Dauw, K.; Vantomme, A.; Welle, A.; Maron, L.; Carpentier, J.-F.; Kirillov, E. Al-alkenyl-induced formation of long-chain branched polyethylene via coordinative tandem insertion and chain-transfer polymerization using $(n\text{BuCp})_2ZrCl_2$/MAO systems: An experimental and theoretical study. *Eur. Polym. J.* **2021**, *154*, 110567. [CrossRef]
31. Nifant'ev, I.E.; Ivchenko, P.V.; Bagrov, V.V.; Churakov, A.V.; Chevalier, R. Novel Effective Racemoselective Method for the Synthesis of ansa-Zirconocenes and Its Use for the Preparation of C2-Symmetric Complexes Based on 2-Methyl-4-aryltetrahydro(s)indacene as Catalysts for Isotactic Propylene Polymerization and Ethylen. *Organometallics* **2012**, *31*, 4340–4348. [CrossRef]
32. Nifant'ev, I.E.; Ivchenko, P.V.; Bagrov, V.V.; Churakov, A.V.; Mercandelli, P. Novel effective racemoselective method for the synthesis of ansa-zirconocenes and its use for the preparation of C2-symmetric complexes based on 2-methyl-4-aryltetrahydro(s)indacene as catalysts for isotactic propylene polymerization and ethylene-propylene copolymerization. *Organometallics* **2012**, *31*, 4962–4970.
33. Chevalier, R.; Garcia, V.; Müller, P.; Sidot, C.; Tellier, C.; Delacray, L. Meso-Selective Synthesis of Ansa-Metallocenes. Patent WO2005058929A1, 15 December 2004.
34. Frisch, M.J.; Trucks, G.W.; Schlegel, H.B.; Scuseria, G.E.; Robb, M.A.; Cheeseman, J.R.; Scalmani, G.; Barone, V.; Mennucci, B.; Petersson, G.A.; et al. *Gaussian 09, Revision D.01*; Gaussian Inc.: Pittsburgh, PA, USA, 2009.
35. Becke, A.D. Density-functional exchange-energy approx- imation with correct asymptotic behavior. *Phys. Rev. A* **1988**, *38*, 3098–3100. [CrossRef]
36. Becke, A.D. Density-Functional Thermochemistry 0.3. The Role of Exact Exchange. *J. Chem. Phys.* **1993**, *98*, 5648–5652. [CrossRef]
37. Marenich, A.V.; Cramer, C.J. Universal Solvation Model Based on Solute Electron Density and on a Continuum Model of the Solvent Defined by the Bulk Dielectric Constant and Atomic Surface Tensions. *J. Phys. Chem. B* **2009**, *113*, 6378–6396. [CrossRef]
38. Castro, L.; Kirillov, E.; Miserque, O.; Welle, A.; Haspeslagh, L.; Carpentier, J.-F.; Maron, L. Are Solvent and Dispersion Effects Crucial in Olefin Polymerization DFT Calculations? Some Insights from Propylene Coordination and Insertion Reactions with Group 3 and 4 Metallocenes. *ACS Catal.* **2015**, *5*, 416–425. [CrossRef]